



日本原子力研究開発機構機関リポジトリ
Japan Atomic Energy Agency Institutional Repository

Title	Chemical state analysis of trace-level alkali metals sorbed in micaceous oxide by total reflection X-ray photoelectron spectroscopy
Author(s)	Baba Yuji, Shimoyama Iwao, Hirao Norie
Citation	Applied Surface Science, 384, p.511-516
Text Version	Author's Post-print
URL	https://jopss.jaea.go.jp/search/servlet/search?5056032
DOI	https://doi.org/10.1016/j.apsusc.2016.05.067
Right	© 2016. This manuscript version is made available under the CC-BY-NC-ND 4.0 license http://creativecommons.org/licenses/by-nc-nd/4.0/



Chemical state analysis of trace-level alkali metals sorbed in micaceous oxide by total reflection X-ray photoelectron spectroscopy

Y. Baba*, I. Shimoyama and N. Hirao

Japan Atomic Energy Agency, Tokai-mura, Naka-gun, Ibaraki, 319-1195, Japan

Abstract

In order to determine the chemical states of radioactive cesium (^{137}Cs or ^{134}Cs) sorbed in clay minerals, chemical states of cesium as well as the other alkali metals (sodium and rubidium) sorbed in micaceous oxides have been investigated by X-ray photoelectron spectroscopy (XPS). Since the number of atoms in radioactive cesium is extremely small, we specially focused on chemical states of trace-level alkali metals. For this purpose, we have measured XPS under X-ray total reflection (TR) condition. For cesium, it was shown that ultra-trace amount of cesium down to about $100 \text{ pg}\cdot\text{cm}^{-2}$ can be detected by TR-XPS. This amount corresponds to about 200 Bq of ^{137}Cs ($t_{1/2}=30.2 \text{ y}$). It was demonstrated that ultra-trace amount of cesium corresponding to radioactive cesium level can be measured by TR-XPS. As to the chemical states, it was found that core-level binding energy in TR-XPS for trace-level cesium shifted to lower-energy side compared with that for thicker layer. A reverse tendency is observed in sodium. Based on charge transfer within a simple point-charge model, it is concluded that chemical bond between alkali metal and micaceous oxide for ultra-thin layer is more polarized than that for thick layer.

*Present address: *Japan Atomic Energy Agency, 7-1 Aza-Omachi, Taira, Iwaki-shi, Fukushima 970-8026, Japan*

1. Introduction

After the accident of the Fukushima Daiichi Nuclear Power Station, which occurred in March 2011, various kinds of anthropogenic radionuclides such as ^{131}I , ^{90}Sr , ^{134}Cs , ^{137}Cs and $^{110\text{m}}\text{Ag}$ which were formed as common fission products by the nuclear fission of ^{235}U were released into the environment. Most of the radionuclides are mainly trapped in geological materials such as soil and clay. At present, the main problem is gamma-rays emitted from ^{137}Cs (or ^{134}Cs) that may cause damages to human health. Although the effect of low-level radiation on human health has not been fully understood, it is important to lower the radiation level in environment as low as possible. And thus, development of a method for cesium decontamination from geological materials becomes insisting.

It is well known that radioactive cesium is mainly trapped in clay minerals among geological materials [1]. It was reported that cesium is strongly trapped at the micaceous oxides in clay, and its adsorption-desorption behavior has been widely investigated [2-10]. Through these works, it has become clear that radioactive cesium, once sorbed in the micaceous oxides, is hard to be released. Knowledge on structure of cesium sorbed in micaceous oxide is required to develop an efficient method for the decontamination.

Various spectroscopic methods have been applied to elucidate the structures of cesium in clay minerals. The coordination number and bond length around cesium in clay have been clarified by X-ray absorption fine structure (XAFS) [11-14]. Also the crystal structure and microstructure of cesium in clay have been elucidated by X-ray diffraction (XRD) and transmission electron microscopy (TEM) [6]. However, the chemical bonding states of cesium, which is the most important factors concerning the adsorption-desorption behavior of cesium, have not been clarified by spectroscopic methods.

X-ray photoelectron spectroscopy (XPS) as well as Auger electron spectroscopy (AES) is one of the suitable methods to elucidate the chemical states of elements adsorbed on solid

surface. In order to determine the chemical states, XPS is superior to AES because core-level chemical shifts are more clearly observed due to low electron backgrounds. Up to now, there have been some XPS investigations on chemical states of cesium sorbed in clay minerals [15-17]. In these works, however, non-radioactive cesium was used as a sample. It should be noted that the number of atoms in radioactive cesium (^{137}Cs or ^{134}Cs) is extremely small compared with that of non-radioactive cesium used in the above experiments. For example, the amount of cesium in 1000 Bq ^{137}Cs ($t_{1/2}=30.2$ y) is only about 500 pg, which is hard to be detected by conventional XPS. There are many methods to analyze ultra-trace amount of elements such as inductively coupled plasma atomic emission spectroscopy (ICP-AES), atomic absorption spectroscopy (AAS), and X-ray fluorescence spectroscopy (XRF). However these elemental analysis methods cannot determine chemical states.

It is known that the chemical behavior of such ultra-trace elements is in many cases different from that of macro quantity. So it is important to analyze the chemical states of ultra-trace amount of cesium in micaceous oxides in order to clarify the real adsorption states of radioactive cesium. In a previous paper, we have reported that XPS under total reflection (TR) shows enhanced surface sensitivity and detects trace amount of cesium adsorbed on oxides [18].

In the present paper, we apply TR-XPS to analyse chemical states of trace-level cesium as well as the other alkali metals (sodium and rubidium) sorbed in micaceous oxides. The chemical states observed by TR-XPS core-level binding energy for ultra-trace amount of alkali metals sorbed in micaceous oxides are discussed on the basis of a simple electrostatic model.

2. Experimental

The micaceous oxide used was a single crystal of artificially synthesized phlogopite (hereafter micaceous oxide is sometimes simply referred to as “mica”) of $10\times 10\times 0.5$ mm purchased from Crystal Base Co., Ltd (Product Code: 3-4959-01). The chemical composition

of the mica was $\text{KMg}_3\text{AlSi}_3\text{O}_{10}\text{F}_2$, and the density was $2.85 \text{ g} \cdot \text{cm}^{-3}$. The sample was cleaved before adsorption of alkali metals.

Alkali metals (sodium, rubidium, and cesium) were sorbed in mica by aqueous solution. Potassium was not investigated in this work because mica contains potassium. The mica was first immersed in $20 \text{ mM} \cdot \text{dm}^{-3}$ alkali-metal chloride solution at pH 7 for one month. Then the mica was dried in air, and introduced into the vacuum chamber for XPS analysis. This sample is referred to as sample #0.

After the XPS measurements, the alkali-metals sorbed micas (sample #0) were washed by five steps to simulate decontamination of radioactive cesium from clay; 1) splashed with water 2 times (sample #1), 2) splashed with water 10 times (sample #2), 3) immersed in distilled water for 30 min (sample #3), 4) immersed in distilled water with supersonic wave for 15 min (sample #4), and 5) immersed in $1 \text{ M} \cdot \text{dm}^{-3}$ acetic acid with supersonic wave for 30 min (sample #5). The washed samples were again measured by XPS.

For XPS measurements, we used soft X-rays emitted from synchrotron light source as an excitation source. X-rays from synchrotron light source are superior to those from X-ray tube because of their extremely high intensity, high collimation, and energy-tunability. Especially, highly collimated nature of synchrotron beam allows us to easily get total reflection condition by rotating the sample.

XPS measurements were performed at the soft X-ray beamline (BL-27A) of the Photon Factory in the High Energy Accelerator Research Organization (KEK-PF). The photon energy was tuned by an InSb(111) double crystal monochromator. The typical photon flux was about $10^{10} \text{ photons} \cdot \text{cm}^{-2} \cdot \text{s}^{-1}$ at the sample position. The size of the X-ray beam was $5 \text{ mmW} \times 10 \text{ mmH}$, which was shaped using variable horizontal and vertical slits. The typical photon energy used was 3000 eV. The energy resolution of the monochromator was 1.4 eV at 3000 eV.

The XPS analysis chamber consisted of a five-axis manipulator, an electron energy analyzer,

and an electron flood gun. The base pressure of the analysis chamber was 1×10^{-8} Pa. The sample was vertically located, and it was rotated around the vertical axis. XPS spectra were measured with hemispherical electron energy analyzer (VSW Co. Class-100). The radius of the analyzer was 100 mm. The pass energy of the spectrometer was set to be 100 eV for wide scan, and 20 eV for narrow scan, respectively. The typical measurement times were 10 min for wide scan and 1 hr for narrow scan.

The top view of the setup for XPS measurements is schematically shown in Fig.1. For normal XPS, the X-rays were irradiated at 35° from the surface and the take-off direction of the photoelectrons was surface normal. In the TR-XPS mode, the incident X-rays were irradiated at grazing angle and the take-off direction of photoelectrons were 55° from the surface.

Now we will estimate the critical angle of the total reflection in the present system. The refractive index n of X-ray in a material is given by the following equation [19],

$$n = 1 - \delta + i\beta \quad (1).$$

The real component δ , called the decrement, is a measure of the dispersion. The imaginal component β is a measure of the absorption. Generally the value of β is negligibly small, so the refractive index is approximated as

$$n \sim 1 - \delta \quad (2).$$

For total reflection, X-rays are irradiated at grazing incidence. In this case, the critical angle θ_c for total reflection is approximated as [19]

$$\theta_c \sim (2 \cdot \delta)^{1/2} \quad (3).$$

The value of δ is 6.59×10^{-5} for mica at 3 keV [20], so we obtain $\theta_c = 0.65^\circ$. Based on the result, the incident X-rays were irradiated at 0.2° from the surface, which was certainly lower than the critical angle of total reflection.

Generally, an XPS measurement of such wide-gap insulator is not possible due to positive charge accumulated at the surface (space-charge effect). In the present experiment, we were able to reduce the space-charge effect by 1) using electron flood gun, 2) measuring cleaved thin film, and 3) using high photon energy (3000 eV). Actually, the XPS spectra were shifted by a few eV to lower kinetic energy (E_K) due to a slight space-charge effect. But the binding energy (E_B) of XPS peak could be calibrated because the value of E_K shift was constant in all energy region. As to the E_B reference of mica, the reported values of O 1s and Si 2p in mica or aluminosilicate are scattered. So in the present study, we tentatively used well established value of O 1s ($E_B=532.6$ eV) in silicon dioxide [21] as an energy reference. Accordingly, the E_B of Si 1s was set to be 1844.2 eV. The absolute E_B values are not important in this paper. Instead, we will concentrate on the relative E_B shifts among the samples.

3. Results

Figure 2 shows the XPS wide-scan spectra of Cs-adsorbed mica (sample #0) for two incident X-ray angles. The solid line shows normal XPS where the X-ray incidence angle was 35° and take-off direction of photoelectrons was surface normal. The dotted line displays TR-XPS, where the X-ray incidence angle was 0.2° and take-off direction of photoelectrons was 55° . The intensity of the two spectra are normalized at the O 1s peak. The spectra around Cs 3d region is displayed in small inset as an expanded energy scale. For normal XPS, the backgrounds around 730 eV, where Cs 3d peaks are located, were in the order of 300 cps due to the inelastically scattered electrons accompanied by the O 1s photoelectron emission. For

TR-XPS, the background in this region is reduced to be lower than 80 cps. This background reduction comes from the fact that the incident X-rays were totally reflected, so the amount of inelastically scattered electrons produced by O 1s photoelectron emission decreased. Owing to the background reduction, trace level cesium down to one-thousandth monolayer could be detected (detection limit will be discussed later).

Figure 3 shows the TR-XPS semi-wide scans for (a) sodium-, (b) rubidium-, and (c) cesium-adsorbed mica. Compared with general XPS using Mg $K\alpha$ ($h\nu=1253.6$ eV) or Al $K\alpha$ ($h\nu=1486.6$ eV) X-rays, high energy photon ($h\nu=3000$ eV) was used in this experiment. This has another advantage for the high sensitivity because photoelectron peaks are not overlapped with the low kinetic-energy background mainly caused by Auger electrons. This situation is seen in Fig. 3(a) for Na 1s and Fig. 3(c) for Cs 3d. For rubidium, the highest photoelectron peak in this energy region is Rb 2p_{3/2} as seen in Fig. 3(b). This peak locates a little higher energy side than that of Si 1s, so the background due to the inelastically scattered Si 1s photoelectron is low. So we will hereafter concentrate on the analysis of Na 1s for sodium, Rb 2p_{3/2} for rubidium and Cs 3d_{5/2} for cesium, respectively.

Next, we will estimate the averaged thickness of adsorbed layer by the intensity of the metal (Na 1s, Rb 3d_{3/2} or Cs 3d_{5/2}) and Si 1s peaks. The intensity ratio of the photoelectron peaks, $I_{\text{Metal}}/I_{\text{Si 1s}}$, is expressed as

$$\frac{I_{\text{Metal}}}{I_{\text{Si 1s}}} = \sigma_{\text{Metal}} \cdot \lambda_{\text{Metal in A}} \cdot n_{\text{Metal}} \cdot \frac{1 - \exp(-d / \lambda_{\text{Metal in A}} \cdot \sin \theta)}{\sigma_{\text{Si 1s}} \cdot \lambda_{\text{Si 1s in S}} \cdot n_{\text{Si}} \cdot \exp(-d / \lambda_{\text{Si 1s in A}} \cdot \sin \theta)} \quad (4)$$

where σ (barn) is photoionization cross section [22] for the respective photoelectron indicated as a subscript, λ (nm) is inelastic mean free path (IMFP) of photoelectrons in the material

indicated as a subscript [23], n is atomic concentration of an element shown as a subscript, d (nm) is the thickness of the adsorbed layer, and θ is the exit angle of photoelectrons measured from the surface ($\theta=55^\circ$ in TR mode). In the subscripts, A and S represent adsorbate and substrate, respectively. As a typical example, a plot for $I_{Cs\ 3d_{5/2}}/I_{Si\ 1s}$ ratio versus thickness d (nm) calculated by equation (4) for cesium-adsorbed mica is shown in Fig. 4. The $I_{Cs\ 3d_{5/2}}/I_{Si\ 1s}$ value for each sample is marked in the plot. It should be noted that the thickness of the layer shown in Fig. 4 is averaged number of layers supposing that the layer is homogeneous.

In the present TR-XPS measurements, we can detect the Cs $3d_{5/2}$ peak for ultra-thin film less than 5×10^{-3} nm (0.5 pm). When the thickness of the detection limit is converted to weight, it was demonstrated that the detection limit of cesium is about $100\text{ pg}\cdot\text{cm}^{-2}$. If all of the cesium is composed of ^{137}Cs ($t_{1/2}=30.2\text{ y}$), this weight corresponds to about 200 Bq of ^{137}Cs . Considering that in Japan the standard limits for radionuclides in most of foods are in the order of $100\text{ Bq}\cdot\text{kg}^{-1}$ and those in soil are in the order of $1000\text{ Bq}\cdot\text{kg}^{-1}$, it is demonstrated that the ultra-trace amount of cesium comparable to the radioactive cesium level can be measured by TR-XPS.

Now we convert the thickness of the layer d (nm) to the number of layers. The definition of monolayer depends on various factors such as crystal structure, density, and molecular (or atomic) radius. In order to avoid this difficulty, we adopt the following definition of monolayer. If the adsorbates have density ρ ($\text{g}\cdot\text{cm}^{-3}$) and molecular (atomic) weight m , the thickness of the monolayer a (nm) is expressed as

$$a^3 = m \cdot 10^{21} / (\rho \cdot n \cdot N_A) \quad (5),$$

where n is the number of atoms in the molecule ($n=1$ for atom), and N_A is the Avogadro number [23]. As a result, we obtain $a=0.35$ for sodium, $a=0.44$ for rubidium, and $a=0.47$ for cesium,

respectively.

The thickness in the number of layers for all alkali-metal samples washed with various conditions is summarized in Fig. 5. For all alkali metals, the number of layers decreases by washing with water more intensely. For the most intensely washed samples (washed with acetic acid, sample #5), no alkali metals were observed. For samples #4 (washed in water using ultrasonic wave), a small amount of alkali metals still remains. The thickness of the layer for rubidium (#4) and cesium (#4) is less than 1/1000 layers. The thickness of the layer for sodium (#4) is about ten times thicker than that for rubidium and cesium, indicating that sodium is more strongly trapped in mica than the other alkali metals.

Figure 6 shows the TR-XPS narrow scans for (a) sodium, (b) rubidium, and (c) cesium for various washing conditions. The spectra for the sample #4 were shown after smoothing by 5 points because of the low count rates. For rubidium, the Rb $2p_{3/2}$ peak for sample #0 splits into two structures. Although the averaged thickness of the layer is about 1 monolayer, the higher binding-energy peaks (marked A) are due to RbCl precipitates, because this peak disappeared after slight washing. So we will not consider the peak A, but will focus on the lower-energy peak. In all spectra, the peak energy depends on the layer thickness.

The core-level energy for three alkali metals are summarized in Fig. 7. In this figure, the chemical shifts are measured from the binding energy for the non-washed samples (sample #0). For sodium, the Na $1s$ binding energy shifts to higher binding-energy with the increase in the degree of washing condition. On the other hand, the tendencies of the energy shifts observed for rubidium and cesium are reverse to that for sodium. The binding energy of Cs $3d_{5/2}$ (Rb $2p_{3/2}$) shifts to lower energy side with the increase in the degree of washing condition.

In Fig. 8, the core-level energy for three alkali metals is plotted as a function of the layer thickness. For cesium, the core-level energy shifts to lower binding-energy side with the decrease in the thickness. For the thinnest sample, the Cs $3d_{5/2}$ energy for 10^{-3} layer shifts to 1.5

eV lower energy side from that for monolayer. On the other hand, the core-level energy of Na $1s$ for sodium shifts to higher binding-energy side with the decrease in the thickness. The tendency of the thickness dependence for rubidium is between those for sodium and cesium, but the energy of Rb $2p_{3/2}$ line shifts slightly to lower energy side with the decrease in the thickness.

4. Discussion

Except for the sample #0 for rubidium, the observed peaks for alkali metals are not due to the alkali metal chloride, because we did not observe any Cl $1s$ peaks in the XPS spectra. Also the intensity of the C $1s$ peak is negligibly small, so the carbon contamination does not affect the peak energy of alkali metals. Another possibility of the observed peak energy is due to the existence of oxides or hydroxides. We cannot exclude this possibility because large oxygen $1s$ peak from mica is observed and it interferes the oxygen $1s$ peaks from oxides and hydroxides. However, we consider that oxides and hydroxides were desorbed by washing because these species adsorbed on surface through van-der-Waals force. So we believe that the trace-level alkali metals exist at the interlayer of the micaceous oxide in an atomic (ionic) state.

Generally, chemical shifts of core-level binding energy in a metal depend on the valence states of the metal. The core-level energy shifts to higher energy side with the increase of the valence charge. However, alkali metals take only mono valence state. So the core-level energy shift of alkali metals cannot be easily explained because it is caused by the other factors such as charge transfer within a simple point-charge model, the long-range electrostatic interactions (Madelung potential), and final-state contributions due to extra-atomic relaxation of the core-hole (screening effect). But the contributions of the latter two factors are small because thin films less than monolayer were measured (Madelung potential can be ignored) and the insulating substrates were used (screening effect is negligible) in the present experiments. We

will qualitatively discuss the origin of the observed binding-energy shifts on the basis of the charge transfer within a simple point-charge model.

When we consider a compound M-X (M: metal, X: counter anion), the higher the polarization of an M-X bond is, the higher the core-level energy of M becomes. Namely, when the δ value in $M^{\delta+}-X^{\delta-}$ bond becomes large, the XPS binding energy of M shifts to higher energy side. This tendency is commonly observed in most of the metals. Actually in the case of sodium, the Na 1s binding energy shifts to higher energy sides with the increase in the electronegativity of the counter anion [21,24,25]. However, this general tendency does not hold for cesium. In the case of cesium, which has a large atomic radius, shows reverse tendency compared with most of the other metals [21,24]. Actually, it was reported that when metallic cesium is oxidized, the binding energy of the Cs $3d_{5/2}$ line shifts to lower energy, in contrast to the other light alkali metals [25-28].

Then, let's go back to Fig. 8. For sodium, the core-level energy of Na 1s shifts to higher binding-energy side with the decrease in the thickness. This means that the chemical bond between sodium and micaceous oxides for thin layer is more polarized than that for thick layer. In other words, the trace amount of sodium sorbed in micaceous oxides is more ionically bonded with the substrate compared with thick layer. For cesium, on the other hand, the core-level energy shifts to lower binding-energy side with the decrease in the thickness. Considering the difference in the tendency of the energy shifts between sodium and cesium as discussed above, the similar nature of the chemical bond between cesium and substrate is deduced. It has been reported that cesium trapped in the interlayer of muscovite is covalently bonded with oxygen by the theoretical calculation using first-principles study based on density-functional theory [29]. For thick layer (thicker than 0.1 monolayer), almost constant binding energy shown in Fig. 8 shows that polarization between cesium and micaceous oxides is weak as reported in ref [29]. For thin layer, on the other hand, the Fig. 8 shows that the chemical bond between ultra-trace

level cesium and micaceous oxides is more polarized than that for thick layer. This means that the ultra-trace amount of cesium sorbed in micaceous oxides is more ionically bonded with the substrate compared with thick layer.

A question may be raised as to why ultra-trace amount of cesium is ionically bonded with the micaceous oxides. At present, we cannot give a definite answer to this phenomenon. However, one plausible reason is as follows. It is well established that the cesium is trapped at the interlayer of micaceous oxides as an ionic state. But for thick layer, the polarization of the chemical bond between cesium and oxides is relaxed and weakened due to the surrounding cesium ions. For ultra-thin layer, on the other hand, adjacent cesium ions are located far away from a cesium ion. Therefore, the relaxation of the polarizability by the surrounding ions is weak, so ionically bonded nature remains only for ultra-thin layer.

Although more detailed analysis of the chemical bonding states is needed from both experimental and theoretical viewpoints, it is suggested that the ionically bonded state of ultra-trace amount of cesium with micaceous oxides is one of the reasons that the radioactive cesium is hard to be released from clay minerals. As to the detection limit of TR-XPS, the present experiments were done using X-rays emitted from bending magnet of synchrotron light source. If we use more highly collimated and intense X-rays such as those from undulator, we can possibly measure further trace level alkali metals.

4. Summary

In order to elucidate the chemical states of radioactive cesium (^{137}Cs or ^{134}Cs) trapped in clay minerals, chemical states of trace amount of cesium as well as the other alkali metals (sodium and rubidium) sorbed in micaceous oxides have been investigated by TR-XPS. For cesium, it was shown that ultra-trace amount of cesium down to about $100 \text{ pg}\cdot\text{cm}^{-2}$ (equal to 200 Bq of ^{137}Cs) can be detected by TR-XPS, demonstrating that the ultra-trace amount of

cesium corresponding to the radioactive cesium level can be measured by TR-XPS. As to the chemical states, it was found that the TR-XPS core-level binding energy for trace-level cesium shifts to lower-energy side compared with that for thicker layer, which is reverse to that observed in sodium. On the basis of the charge transfer within a simple point-charge model, it is concluded that the chemical bond between alkali metals and micaceous oxide for ultra-thin layer is more polarized than that for thick layer.

Acknowledgements

The authors would like to thank the staff of the KEK-PF for their assistance throughout the experiments. The work has been conducted under the approval of Photon Factory Program Advisory Committee (PF-PAC 2014G096).

References

- [1] J.S. Wahlberg, M.J. Fishman, Ion exchange on mineral materials; Bulletin (Geological Survey (U.S.)), Govt. Print. Off., Washington D.C. 1962.
- [2] T. Tamura, D.G. Jacobs, Structural implications in cesium sorption, Health Physics 2 (1960) 391-398.
- [3] R.N.J. Comans, M. Haller, P.D. Preter, Sorption of cesium on illite: none-equilibrium behaviour and reversibility, Geochim. Cosmochim. Acta 55 (1991) 433-440.
- [4] Y. Kim, R.J. Kirkpatrick, R.T. Cyganet, ^{133}Cs NMR study of cesium on the surfaces of kaolinite and illite, Geochim. Cosmochim. Acta 60 (1996) 4059-4074.
- [5] K. Morimoto, T. Kogure, K. Tamura, S. Tomofuji, A. Yamagishi, H. Sato, Desorption of Cs^+ ions intercalated in vermiculite clay through cation exchange with Mg^{2+} ions, Chem. Lett. 41 (2012) 1715-1717.
- [6] T. Kogure, K. Morimoto, K. Tamura, H. Sato, A. Yamagishi, XRD and HRTEM evidence

- for fixation of cesium ions in vermiculite clay, *Chem. Lett.* 41 (2012) 380-382.
- [7] M. Okumura, H. Nakamura, M. Machida, Mechanism of strong affinity of clay minerals to radioactive cesium: First-principles calculation study for adsorption of cesium at frayed edge sites in muscovite, *J. Phys. Soc. Jpn.* 82 (2013) 033802.
- [8] L. Dzene, E. Tertre, F. Hubert, E. Ferrage, Nature of the sites involved in the process of cesium desorption from vermiculite, *J. Colloid Interface Sci.* 455 (2015) 254-260.
- [9] A.J. Fuller, S. Shaw, M.B. Ward, S.J. Haigh, J.F.W. Mosselmans, C.L. Peacock, S. Stackhouse, A.J. Dent, D. Trivedi, I.T. Burke, Caesium incorporation and retention in illite interlayers, *Applied Clay Science* 108 (2015) 128-134.
- [10] L.K. Zaunbrecher, R.T. Cygan, W.C. Elliott, Molecular models of cesium and rubidium adsorption on weathered micaceous minerals, *J. Phys. Chem. A.* 119 (2015) 5691-5700.
- [11] K.M. Kemner, D.B. Hunter, P.M. Bertsch, J.P. Kirkland, W.T. Elam, Determination of site specific binding environments of surface sorbed cesium on clay minerals by Cs-EXAFS, *J. Phys. IV France* 7 (1997) C2-777-C2-779.
- [12] B.C. Bostick, M.A. Vairavamurthy, K.G. Karthikeyan, J. Chorover, Cesium adsorption on clay minerals: An EXAFS spectroscopic investigation, *Environ. Sci. Technol.* 36 (2002) 2670-2676.
- [13] H. Qin, Y. Yokoyama, Q. Fan, H. Iwatani, K. Tanaka, A. Sakaguchi, Y. Kanai, J. Zhu, Y. Onda, Y. Takahashi, Investigation of cesium adsorption on soil and sediment samples from Fukushima Prefecture by sequential extraction and EXAFS technique, *Geochem. J.* 46 (2012) 297-302.
- [14] D. Matsumura, T. Kobayashi, Y. Miyazaki, Y. Okajima, Y. Nishihata, T. Yaita, Real-time-resolved X-ray absorption fine structure spectroscopy for cesium adsorption on some clay minerals, *Clay Science* 18 (2014) 99-106.
- [15] Y. Kim, R.T. Cygan, R.J. Kirkpatrick, ¹³³Cs NMR and XPS investigation of cesium

- adsorbed on clay minerals and related phases, *Geochim. Cosmochim. Acta* 60 (1996) 1041-1052.
- [16] T. Ebina, T. Iwasaki, Y. Onodera, A. Chatterjee, A comparative study of DFT and XPS with reference to the adsorption of caesium ions in smectites, *Comput. Mater. Sci.* 14 (1999) 254-260.
- [17] N.C. Dutta, T. Iwasaki, T. Ebina, H. Hayashi, A combined X-ray photoelectron and Auger electron spectroscopic study of cesium in variable-charge montmorillonites, *J. Colloid Interface Sci.* 216 (1999) 161-166.
- [18] Y. Baba, I. Shimoyama, N. Hirao, T. Izumi, Interaction between ultra-trace amount of cesium and oxides studied by total-reflection X-ray photoelectron spectroscopy, *e-J. Surf. Sci. Nanotech.* 13 (2015) 417-421.
- [19] A. Bohlen, Total reflection X-ray fluorescence and grazing incidence X-ray spectrometry — Tools for micro- and surface analysis. A review, *Spectrochim. Acta Part B: Atomic Spectroscopy* 64 (2009) 821.
- [20] The Center for X-Ray Optics, Lawrence Berkeley National Laboratory's (LBNL) Materials Sciences Division, Homepage http://henke.lbl.gov/optical_constants/
- [21] C.D. Wagner, W.M. Riggs, L.E. Davis, J.F. Moulder, G.E. Mullenberg, *Handbook of X-ray photoelectron spectroscopy*, Perking-Elmer Corp. MN, USA, 1979.
- [22] J. H. Scofield, *Theoretical Photoionization Cross Section from 1 to 3000eV*, Lawrence Livermore Laboratory, California, 1973.
- [23] M.P. Seah, W.A. Dench, Quantitative electron spectroscopy of surfaces: A standard data base for electron inelastic mean free paths in solids, *Surf. Interface Anal.* 1 (1979) 2.
- [24] H. Estrade-szwarczkopfa, B. Rousseaua, C. Heroldb, P. Lagrangeb, Sodium - oxygen graphite intercalation compound: XPS, UPS and STM study, *Mol. Cryst. Liquid Cryst. Sci. Tech. Sec. A.* 310 (1998) 231-236.

- [25] M. Ayyoob, M.S. Hegde, An XPS study of the adsorption of oxygen on silver and platinum surfaces covered with potassium or cesium, *Surf. Sci.* 133 (1983) 516-532.
- [26] V.I. Bukhtiyarov, I.P. Prosvirin, R.I. Kvon, B.S. Bal'zhinimaev, E.A. Podgornov, XPS and TPD studies of C-O complexes on Ag surfaces: single crystal versus supported catalysts, *Appl. Surf. Sci.* 115 (1997) 135-143.
- [27] E.A. Podgornov, I.P. Prosvirin, V.I. Bukhtiyarov, XPS, TPD and TPR studies of Cs-O complexes on silver: their role in ethylene epoxidation, *J. Mol. Catal. A: Chemical* 158 (2000) 337-343.
- [28] D. Krix, H. Nienhaus, Low-temperature oxidation of alkali overlayers: Ionic species and reaction kinetics, *Appl. Surf. Sci.* 270 (2013) 231-237.
- [29] M. Okumura, H. Nakamura, M. Machida, First-principles studies on cesium adsorption of clay minerals; Mechanism and chemical bonding (in Japanese), *J. Atomic Energy Soc. Jpn.* 56 (2014) 20-25.

Figure captions

- Fig. 1 Top view of setup for XPS measurements.
- Fig. 2 XPS wide scan spectra for cesium-adsorbed micaceous oxide. Solid line shows the normal XPS, and dotted line represents the TR-XPS. Photon energy was 3000 eV. Intensity of the two spectra are normalized at the O 1s peaks. In the small inset, semi-wide scan spectra around Cs 3d region are shown in an expanded energy scale.
- Fig. 3 TR-XPS wide scan spectra for (a) sodium-adsorbed, (b) rubidium-adsorbed, and (c) cesium-adsorbed micaceous oxide. Photon energy was 3000 eV.
- Fig. 4 Relation between photoelectron intensity ratio ($I_{Cs3d5/2}/I_{Si1s}$) and thickness of the layer for cesium-adsorbed micaceous oxide. Solid line represents the calculated value on the basis of the equation (1). The experimental values for cesium-adsorbed micaceous oxide before washing (#0) and after various washing procedures (#1~#4) are indicated in the figure.
- Fig. 5 Thickness of layer for sodium, rubidium, and cesium adsorbed on mica before washing (#0) and after various washing procedures (#1 ~ #4). The washing procedures are described in the experimental section in the text.
- Fig. 6 TR-XPS narrow scan spectra for (a) sodium, (b) rubidium, and (c) cesium, adsorbed on mic before washing (#0) and after various washing procedures (#2~#4). The washing procedures are described in the experimental section in the text. Photon

energy was 3000 eV. The spectra of #4 samples are shown after smoothing.

Fig. 7 Core-level binding energy shifts (E_B shift) for sodium, rubidium, and cesium adsorbed on mica before washing (#0) and after various washing procedures (#1~#4). The washing procedures are described in the experimental section in the text. The E_B shifts were measured from the E_B values for the sample #0 of respective metals, i.e., 1071.8 eV for Na $1s$, 1804.6 eV for Rb $2p_{3/2}$, and 725.3 eV for Cs $3d_{5/2}$.

Fig. 8 Core-level binding energy shifts (E_B shift) for sodium, rubidium, and cesium adsorbed on mica as a function of the thickness. The E_B shifts were measured from the E_B values for the sample #0 of respective metals, i.e., 1071.8 eV for Na $1s$, 1804.6 eV for Rb $2p_{3/2}$, and 725.3 eV for Cs $3d_{5/2}$.

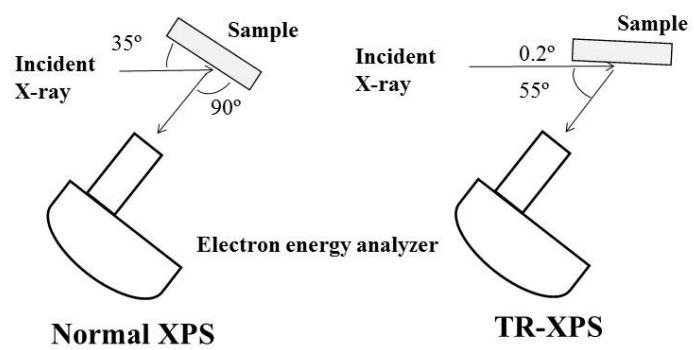


Fig. 1

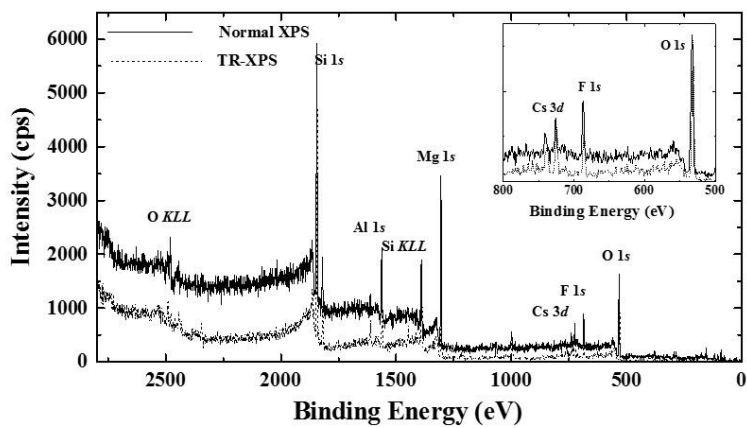


Fig. 2

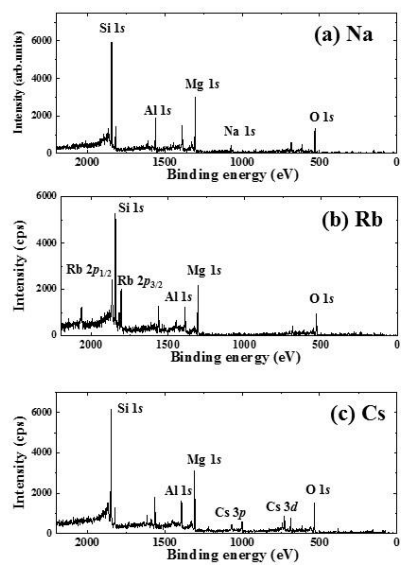


Fig. 3

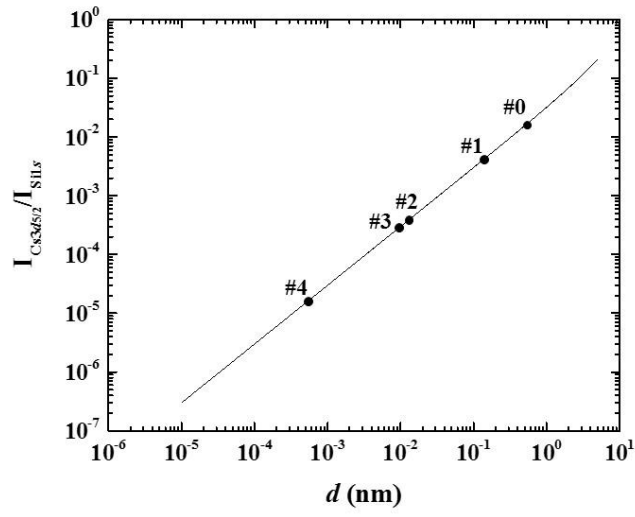


Fig. 4

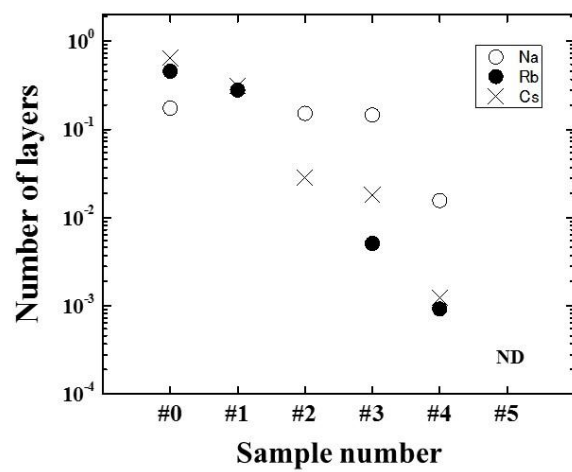


Fig. 5

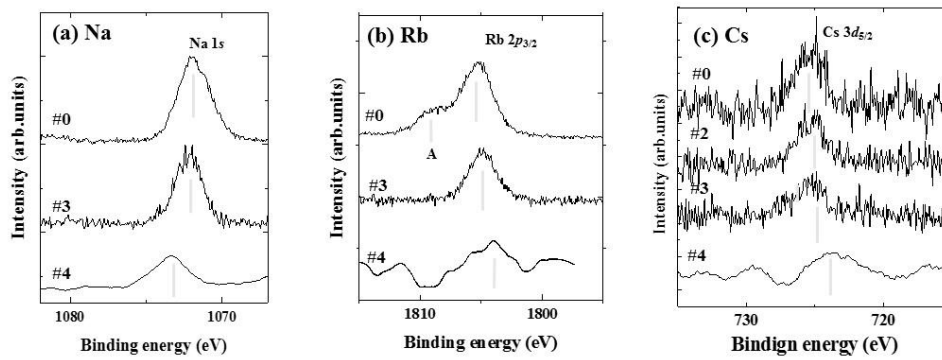


Fig. 6

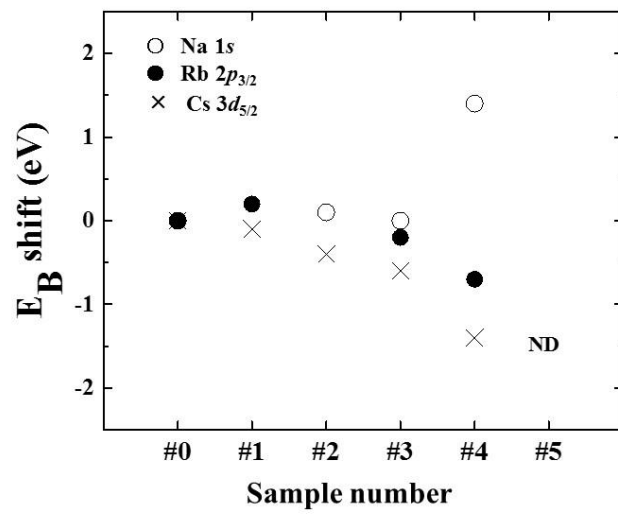


Fig. 7

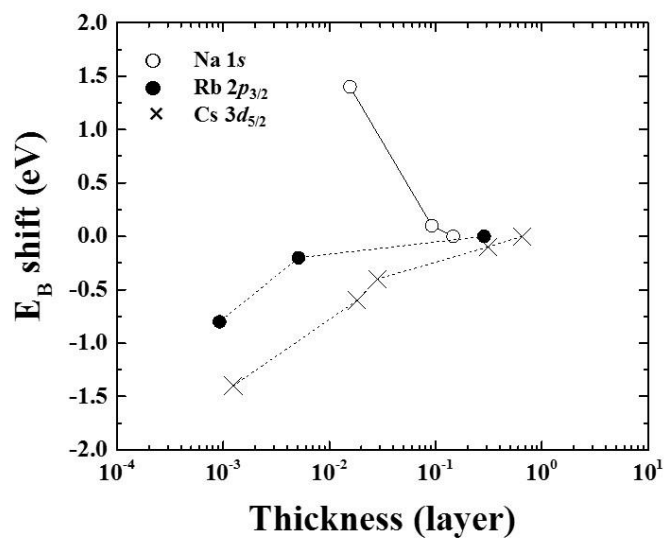


Fig. 8